Biochimica et Biophysica Acta 1843 (2014) 2705–2718

Contents lists available at ScienceDirect

Biochimica et Biophysica Acta

journal homepage: www.elsevier.com/locate/bbamcr

Expression of sarco (endo) plasmic reticulum calcium ATPase (SERCA) system in normal mouse cardiovascular tissues, heart failure and atherosclerosis

Larissa Lipskaia [a,b,c], Zela Keuylian [d,e,1], Karl Blirando [d,1], Nathalie Mougenot [f], Adeline Jacquet [f], Clotilde Rouxel [d], Haifa Sghairi [g,h], Ziane Elaib [g,h], Regis Blaise [d], Serge Adnot [b,c], Roger J. Hajjar [a], Elie R. Chemaly [a,i], Isabelle Limon [d], Regis Bobe [g,h,*]

[a] Mount Sinai School of Medicine, Cardiovascular Research Center, NY, USA
[b] Inserm, U955, Equipe 8, Créteil, France
[c] Université Paris-Est, Faculté de médecine, Créteil, France
[d] Sorbonne Universités, UPMC Univ Paris 06, CNRS, UMR 8256 B2A, IBPS, F-75005, Paris, France
[e] INSERM U1155, Tenon Hospital, Paris, France
[f] PECMV, IFR14, Paris 6, France
[g] INSERM U770, Le Kremlin-Bicetre, France
[h] Université Paris-sud, Le Kremlin-Bicetre, France
[i] Department of Biomedical Engineering, University of Virginia, School of Medicine, Charlottesville, VA, USA

ARTICLE INFO

Article history:
Received 6 May 2014
Received in revised form 29 July 2014
Accepted 1 August 2014
Available online 7 August 2014

Keywords:
Ca^{2+}ATPase
SERCA
Calcium signaling
Cardiovascular
Heart
Smooth muscle cells

ABSTRACT

The sarco(endo)plasmic reticulum Ca^{2+}ATPases (SERCA) system, a key regulator of calcium cycling and signaling, is composed of several isoforms. We aimed to characterize the expression of SERCA isoforms in mouse cardiovascular tissues and their modulation in cardiovascular pathologies (heart failure and/or atherosclerosis).

Five isoforms (SERCA2a, 2b, 3a, 3b and 3c) were detected in the mouse heart and thoracic aorta. Absolute mRNA quantification revealed SERCA2a as the dominant isoform in the heart (~99%). Both SERCA2 isoforms co-localized in cardiomyocytes (CM) longitudinal sarcoplasmic reticulum (SR), SERCA3b was located at the junctional SR. In the aorta, SERCA2a accounted for ~91% of total SERCA and SERCA2b for ~5%. Among SERCA3, SERCA3b was the most expressed (~3.3%), mainly found in vascular smooth muscle cells (VSMC), along with SERCA2a and 2b.

In failing CM, SERCA2a was down-regulated by 2-fold and re-localized from longitudinal to junctional SR. A strong down-regulation of SERCA2a was also observed in atherosclerotic vessels containing mainly synthetic VSMCs. The proportion of both SERCA2b and SERCA3b increased to 9.5% and 8.3%, respectively.

In conclusion: 1) SERCA2a is the major isoform in both cardiac and vascular myocytes; 2) the expression of SERCA2a mRNA is ~30 fold higher in the heart compared to vascular tissues; and 3) nearly half the amount of SERCA2a mRNA is measured in both failing cardiomyocytes and synthetic VSMCs compared to healthy tissues, with a relocation of SERCA2a in failing cardiomyocytes. Thus, SERCA2a is the principal regulator of excitation–contraction coupling in both CMs and contractile VSMCs.

1. Introduction

Ca^{2+} homeostasis plays a pivotal role in cardiovascular contractile function. Among various Ca^{2+} transporters, the calcium pumps sarco/endoplasmic reticulum Ca^{2+}ATPase (SERCA) is the only active Ca^{2+} transporter in the sarcoplasmic reticulum (SR). In muscular cells, SERCA controls the SR Ca^{2+} store that can be mobilized during muscle contraction and it decreases cytosolic Ca^{2+} concentration to allow muscle relaxation. However, Ca^{2+} signaling is complex and several SERCA proteins have been described in human cardiomyocytes [1]. Regulation of their function is a key mechanism controlling not only contractile function, but also protein expression and cellular differentiation through excitation/transcription coupling [2].

The growing family of SERCA is coded by 3 *ATP2A1-3* genes located on different chromosomes, encoding for SERCA1, SERCA2 and SERCA3 isoforms respectively; further diversity is generated by alternative splicing [3]. Isoform expression is also specific to cell-type and developmental stage [3].

* Corresponding author at: INSERM U770, Le Kremlin-Bicetre, France. Tel.: +33 1 49 59 56 40; fax: +33 1 46 71 94 72.
E-mail address: regis.bobe@inserm.fr (R. Bobe).
[1] Both authors contribute equally to the manuscript.

http://dx.doi.org/10.1016/j.bbamcr.2014.08.002
0167-4889/

The SERCA1 gene encodes for 2 spliced mRNA variants (adult (a) and fetal (b)), mostly expressed in fast-twitch skeletal muscle [3].

The SERCA2 gene gives rise to four species (a–d) through alternative splicing of the SERCA2 gene [1]. The so-called "cardiac isoform" SERCA2a, is expressed in cardiac muscle, slow-twitch skeletal muscle and smooth muscle cells, while SERCA2b is a ubiquitous isoform expressed in muscle and non-muscle cells [3]. SERCA2a and SERCA2b are produced by alternative splicing of the SERCA gene and differ only by the replacement of the last 4 amino acids of SERCA2a by an additional 49 amino acids in SERCA2b, possibly coding for an additional trans-membrane loop in the SR [4].

SERCA3 has various 3′-end spliced variants encoding the common SERCA3a isoform [5], in addition to species-specific isoforms, including 5 human (SERCA3b-f) [5–7], 2 mouse (SERCA3b-c) [8] and 1 rat (SERCA3b/c) proteins [9]. SERCA3 isoforms are mostly expressed in non-muscle cells, especially in endothelial and hematopoietic cells, with minor expression in muscle cells [3].

At least 14 different SERCA mRNA variants have been identified with their corresponding proteins. Some of these isoforms are specific to humans; to date, SERCA2c, SERCA2d, SERCA3d, SERCA3e and SERCA3f [1].

As all the members of the SERCA family share the same efficiency (transport of two Ca^{2+} ions per ATP), SERCA isoforms functionally differ only by their affinity for Ca^{2+} ($2b > 2a = 1 > 2c > 3$) and their Ca^{2+} transport turn-over rates, SERCA2b having the lowest transport capacity among all SERCA isoforms [3,10–12]. In-vitro functional characterization of the main muscular SERCA isoforms clearly indicated that SERCA2a displays a lower affinity for Ca^{2+} but has a higher turnover rate compared to SERCA2b. SERCA3 isoforms are characterized by an even lower Ca^{2+} affinity but a rapid turnover rate [13].

Several SERCA isoforms have been described in the cardiovascular system (reviewed in [14]), particularly in human cardiomyocytes [1]. At least 6 SERCA isoforms: SERCA2a, 2b, 2c and SERCA3a, 3d and 3f have been described in human cardiomyocytes with distinct intracellular localization [1]. Of note, in the mouse and human adult heart, SERCA2a was described as the major cardiac isoform, while SERCA2b appeared as the minor one [1,15].

In vascular smooth muscle cells from the rat thoracic aorta, SERCA2a and SERCA2b mRNA were shown to account respectively for 30% and 70% of total SERCA2 mRNA [16], and expression of other isoforms was not reported. It is well established that SERCA2a is down-regulated during pathologic cardiac hypertrophy and heart failure, and its down-regulation is associated with impaired calcium cycling, as previously reviewed in detail [17]). A similar down-regulation of SERCA2a was observed during vascular proliferative remodeling (reviewed in [18,19]). Restoration of SERCA2a expression by gene transfer improves various features of heart failure in preclinical models and in phase 1 and phase 2 clinical trials [20,21]. It also prevents VSMC proliferation in animal models of restenosis after vascular injury [18]. Altogether, present studies demonstrate that the physiological role of SERCA2a in muscle cells is to regulate "contractile" calcium cycling.

The physiological roles of other isoforms detected in the heart (SERCA2b, SERCA2c and various SERCA3 family members (3a, 3d and 3f)) remain unclear [1,11,22]. Reduced SERCA expression and activity are recognized as a major event in cardiomyocyte hypertrophy and vascular proliferative remodeling. However, the existence of a physiological and pathophysiological interplay between various SERCA isoforms, potentially forming a system, has not been investigated. Therefore, we aimed to characterize the expression and the cellular localization of the SERCA isoform system in normal mouse cardiomyocytes, vascular smooth muscle and endothelial cells (referred to respectively as CM, VSMC, EC) and in mouse models of heart failure and atherosclerosis.

2. Material and methods

2.1. Animal models

2.1.1. Model of heart failure

Eight week old C57BL/6 male mice were purchased from Janvier (CERJ, Saint Berthevin, France). Animals were housed at 5 per cage under controlled environmental conditions, with 12 h light:dark cycle at 22 °C of controlled temperature, food and water ad libitum. Animal experiments were conducted in agreement with our institutional guidelines for the use of animals in research.

Mice were anesthetized by intraperitoneal injection of pentobarbital sodium (50 mg/kg), intubated, and mechanically ventilated with 100% oxygen via a positive pressure respirator (Minivent type 845, Hugo Sachs, Elektronik-Harvard Apparatus, Germany). The ventilation rate was 170 strokes per minute, and the tidal volume was 200 μl. Body temperature was maintained at 37 °C. A left thoracotomy was performed in the fourth intercostal space to induce left ventricular infarction (myocardial infarction, MI) by ligation of the left anterior descending coronary with an 8-0 Prolene, or for a sham operation (Sham). The chest was closed in layers. Myocardial ischemia was confirmed by the occurrence of regional blanching.

Echocardiographic examination was performed under isoflurane sedation, using the echocardiography-Doppler (General Electric Medical systems Co, Vivid 7 Dimension/Vivid 7 PRO) with a probe emitting ultrasounds with 9–14 MHz frequency. Two-dimensional images and M-mode measurements were used to quantify left ventricular dimension and function. At least three sets of measures were obtained from three different cardiac cycles. Echocardiography was performed at 1 month and 6 months after MI. At 6 months, the animals were sacrificed and the heart was removed for morphometric analysis and tissue sampling.

2.1.2. Model of atherosclerosis

$ApoE^{-/-}$ mice were purchased from Charles River. Mice were housed under a 12-hour light/12-hour dark cycle (relative humidity: 55–60%; temperature: 22 °C) and were given standard chow and water ad libitum. At 48 weeks of age, male mice were sacrificed by a lethal dose of pentobarbital (intra-peritoneal injection) and heart tissues with attached aortic roots and aortas were collected. Aortas were immediately dissected, snap frozen in RNA later (Ambion) and stored at −80 °C for subsequent RNA extraction. Heart tissues were fixed in 4% formalin for 1 h then soaked in 20% glucose overnight. Tissues were frozen and stored at −80 °C.

2.2. Ultrasound biomicroscopy of atherosclerosis lesions in the brachiocephalic arteries

Images were acquired of the brachiocephalic artery every 3 weeks in mice starting from 30 weeks of age up to 48 weeks. Prior to ultrasound examination, all mice were anesthetized with 3% isoflurane gas and maintained lightly anesthetized with an isoflurane dose of 1.5% during analysis (Minerve Veterinary Equipment, France). The hair of the anterior chest wall was removed and ultrasound transmission gel was applied liberally before scanning. Ultrasound examinations were performed using the Ultrasound Biomicroscope (VEVO 2100, Visualsonics, Toronto) with a 40 MHz probe (MS550D). The Ultrasound Biomicroscope allows real time in vivo observations at high resolution (90 and 40 μM lateral and axial resolution, respectively) using a high frequency transducer (40 MHz). Real time visualization was assessed at 60 images/s. Images were taken in B-mode, or 2 dimensional mode. The probe was positioned in a right parasternal and longitudinal long- and short-axis view at the level of the ascending aorta. More specifically, the location transducer was at the lower 1/3rd of the chest; the direction of the transducer was posterior and leftward, 70° with the coronal plane; the orientation of the imaging plane was parallel to the central axis of

the mouse's body. Proximal and distal plaque areas were defined respectively as the plaque close to the aortic root and the plaque close to the bifurcation of the left subclavian artery. The long axis view in B-mode was used to the bifurcation of the left subclavian artery. The long axis view in B-mode was used to measure the total atherosclerotic plaque surface (mm^2); lesions visualized in the superior and inferior portion of the brachiocephalic artery were outlined and measured by VEVO2100 software. The image chosen from each ultrasonographic sequence corresponds to the one representing the largest detected atherosclerotic plaque for all mice.

2.3. RNA extraction of aortas

Tissues were thawed and homogenized in an Ultrathurax mechanical homogenizer. mRNA was extracted using the standard Trizol protocol (Life Technologies) until phase separation. RNA precipitation was performed using the RNeasy Midi Kit (Qiagen) according to the manufacturer's instructions, in order to optimize RNA collection and reduce the risk of contamination by organic solvents. RNA quality was determined by agarose gel electrophoresis with ethidium bromide; the 18S and 28S RNA bands were visualized under UV light.

2.4. Histological analysis

Cardiac fibrosis was determined by Sirius red staining by using a Picrosirius Red Stain Kit (Polysciences Inc.). Cryosections were fixed in Bouin's solution (1 h, 56 °C), then stained with Sirius red. Collagen fibers in the heart stained a red color and the cardiac fibrotic area was evaluated using ImageJ software. Cardiac fibrosis was quantified including the infarct scar. The size of cardiomyocytes was evaluated on cross sections using Wheat germ agglutinin (WGA) Alexa Fluor® 488 conjugate (Invitrogen).

2.5. Real-time quantitative reverse transcription–polymerase chain reaction (RT-PCR) assays

Relative gene expression was determined using two-step quantitative real-time PCR. Total RNA was isolated with TRIzol reagent (Invitrogen) followed by a cleanup step as described in the RNeasy Isolation kit (Qiagen) with on-column DNase I treatment to eliminate contaminating genomic DNA with RNase-free DNase Set (Qiagen). After annealing oligodT (1 μM) to template RNAs (0.5 μg) at 70 °C for 5 min, primer extension was initiated by adding the RT-MMLV enzyme plus 0.5 mM dNTP, 1U RNAsin and 10 mM dithiothreitol (DTT), and carried out for 45 min at 37 °C. Quantitative PCR was performed using the Light Cycler LC480 (Roche Diagnostics). The PCR mix included 5 μl of each reverse transcriptase (diluted 1:25) and 300 nM of each primer in 1 × Light Cycler DNA SYBR Green 1 Master Mix. The forward and reverse primer sequences for complementary DNA (cDNA) of mouse genes (Table 1) were designed with Primer Express software according to European Molecular Biology Laboratory accession numbers.

PCRs were performed using the following thermal settings: denaturation and enzyme activation at 95 °C for 5 min, followed by 40 cycles of 95 °C (10 s), 60 °C (15 s), and 72 °C (15 s). Post-amplification dissociation curves were performed to verify the presence of a single amplification product and the absence of primer dimers. Controls and water blanks were included in each run; they were negative in all cases. Relative expression of a target gene (SERCA) was standardized by a non-regulated reference gene (GAPDH or calsequestrin). Real-time quantitative PCR data represent the amount of each target messenger RNA (mRNA) relative to the amount of GAPDH gene mRNA or cardiac calsequestrin gene mRNA, estimated in the logarithmic phase of the PCR. Each specific cDNA amplicon was purified and serial dilutions of determined concentration were used to determine the fit coefficients of the relative standard curve. Absolute quantification of SERCA mRNA was performed by interpolation of its PCR signal (Cq) into this standard curve using the Livak-Schmittgen equation: Quantity $= 10^{(Cq - b) / m}$, where b is the y-intercept and m is the slope of the linear regression [23].

2.6. Protein analysis

Immunoblots were performed according to a standard protocol. Immunolabelings were performed on acetone-fixed sections according to a standard protocol. The following SERCA primary antibodies were used: anti-SERCA2a and anti-SERCA2b were from affinity Bioreagent, the anti-SERCA2c was directed against the corresponding human peptide (YLEPVLSSEL) that is mostly preserved in the potential mice SERCA2c terminal part (YLEQPVLSLEP) and was produced by Eurogentec. The anti-SERCA3a (C90) was raised against the rat sequence LSRHHVDEKKDLK that is nearly similar to the mice sequence LSRNHMDEKKDLK, anti-SERCA3b was specifically raised against the mice peptide TGKKGPEVNPNPGSRGES, and the anti-SERCA3c was directed against the human C-Terminal peptide of SERCA3c; HTGLASLKK that is also very close to the C-terminal part of the mice SERCA3c: HTGLASWKKRT. [1,7]. The other primary antibodies used were purchased from Santa Cruz Biotechnology: anti-glyceraldehyde 3-phosphate dehydrogenase (GAPDH) (sc-47424), anti-calsequestrine (sc-28274) and anti-desmin (sc-271677) and anti-PECAM (sc-1506).

2.7. Confocal immunofluorescence microscopy

Immunostaining was performed using the described upper primary antibodies and secondary antibodies conjugated to Alexa-546 or Alexa-488. Slides were examined with a Leica TCS4D confocal scanning laser microscope equipped with a 25 mW argon laser and a 1 mW helium-neon laser, using a Plan Apochromat 63× objective (NA 1.40, oil immersion). Green fluorescence was observed with a 505–550 nm band-pass emission filter under 488 nm laser illumination.

Table 1
The forward and reverse primer sequences for complementary DNA (cDNA) of mouse genes.

	Forward	Reverse
SERCA2a	CTCCATCTGCTTGTCCAT	GCGGTTACTCCAGTATTG
SERCA2b	CTCCATCTGCTTGTCCAT	GGCTGCACACACTCTTTAC
SERCA2c	CTCCATCTGCTTGTCCAT	CTAAGGCTCTAAGTCGAGAA
SERCA3	GGGGTGGTGCTTCAGATGTCTCTGC	GGGGACCCTCCTGTGCTGGCTGGCC
SERCA3a	GGGGTGGTGCTTCAGATGTCTCTGC	CCTTTTTTTCATCCATGTGATTCC
SERCA3b	GGGGTGGTGCTTCAGATGTCTCTGC	CCTTTTTTTCCGGTGTGGTATGG
SERCA3c	GGGGTGGTGCTTCAGATGTCTCTGC	TTTTCCAAGAAGCCAACCCGG
GAPDH	ACA CAT TGG GGG TAG GAA CA	AAC TTT GGC ATT GTG GAA
Calsequestrine	CCT TTG AGC GCA TCG AG	GAT GTA AGG CTG GAA GTG T
E-selectin	AGG GCT TTA GCT TGC AT	CGT CAA GGC TTG GAC ATT
MHC	GGC TTC ATT TGT TCC TTC CA	GGA GCG TCC ATT TCT TCT TC
SM22	TAT GGC AGC AGT GCA GAG	CTT TCT TCA TAA ACC AGT TGG GA
Smoothelin	TCT CAA CAG CGA GAA GC T GA	TGG TCA ACT CCT CGA CAT CA

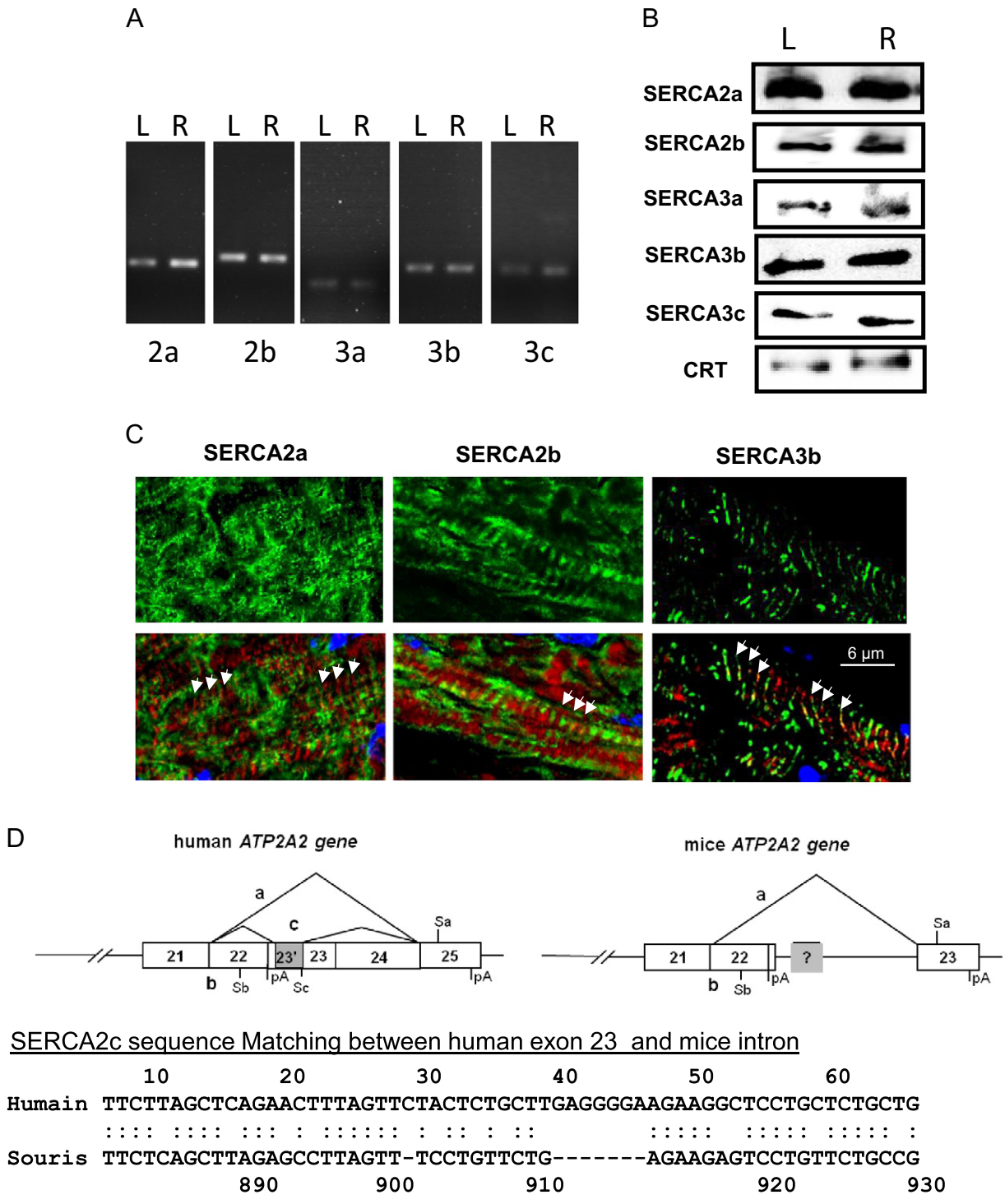

Fig. 1. Endogenous expression of SERCA 2 & 3 isoform mRNA and proteins in normal mouse heart. Expression of the different SERCA isoforms was assessed either by RT-PCR (**A**) or by immunodetection (**B**) in left (L) or right (R) ventricle. The amount of protein loads in each well was controlled using detection of calreticulin (CRT) as indicated in methods. **C**. Localization of the three major SERCA isoforms (green) within the cardiomyocytes (longitudinal sections from left ventricle). Confocal immunofluorescence. Red—F-actin, phalloidin staining. Arrows indicate the position of I-band. **D.** Schematic representation of human and mice ATP2A2 gene and comparison between human cDNA exon 23 with the hypothetical mice analog.

Red fluorescence was observed with a 560 nm long-pass emission filter under 543 nm laser illumination. Pinholes were set at 1.0 airy units. Stacks of images were collected every 0.4 µm along the z-axis. All settings were kept constant to allow comparison. For double immunofluorescence, dual excitation using the multitrack mode (images taken sequentially) was achieved using the argon and He/Ne lasers.

2.8. Statistical analysis

All quantitative data are presented as mean of at least 3 independent experiments ± SEM. One-way ANOVA tests were performed for comparisons between multiple groups. Statistical comparisons of 2 groups were done by an unpaired Student's *t*-test. Differences were considered significant for $P < 0.05$.

3. Results

3.1. Identification of SERCA isoforms expressed in normal mouse cardiovascular tissues

The SERCA system of the mouse heart was first characterized in normal C57-BL/6 mice by RT-PCR and western blot (Fig. 1A & B). RT-PCR analysis revealed the expression of at least 5 SERCA isoforms in the left and right ventricles: 2a, 2b, 3a, 3b and 3c (Fig. 1A). No SERCA2c mRNA was found in mice, while a corresponding sequence displaying 66.7% of similarity for a score 96, was identified in the mouse SERCA2 gene (Fig. 1D). Expression of these isoforms in the heart at the protein level was also confirmed by immunoblot analysis (Fig. 1B). Absolute quantitative real-time PCR shows SERCA2a to be the major cardiac isoform (~99.9%) whereas the ubiquitous SERCA2b represents less than 0.1% of total SERCA mRNA (Table 2). SERCA3 transcript variants were all expressed at very low levels compared to SERCA2a and SERCA2b. As shown in immunofluorescent images (Fig. 1C), i) SERCA2a was located in the longitudinal reticulum of cardiomyocytes, in opposite phase to the position of the I-band (F-actin) indicated by phalloidin staining; ii) SERCA2b demonstrated sub-compartmental localization and a uniform distribution similar to SERCA2a. In contrast, the third cardiac isoform SERCA3b co-localized with the I-bands (Fig. 1C), suggesting an expression preferentially in the junctional reticulum, near Z-band and traversal tubules. No specific localization for minor SERCA isoforms (SERCA3a and 3c) was clearly observed in cardiomyocytes, suggesting that these isoforms are more specific to vascular cells.

The same isoforms were identified by RT-PCR analysis in WT mouse aorta, but their relative expressions were different compared to the heart (Table 2). SERCA2a appeared, once again, as the major isoform in the normal aorta, but its expression is much lower than in the heart (~30 pg/μg of RNA in aorta vs ~920 pg/μg of RNA in the heart). Although SERCA2b expression was 0.86 and 1.6 pg/1 μg of total RNA in the heart and aorta respectively, the percentage of SERCA2a still represented more than 90% of total SERCA, and that of SERCA2b isoform ~5%. Expression of SERCA3b is higher in the aorta than in heart, respectively 1.01 ± 0.21 pg/μg RNA and 0.19 ± 0.07 pg/μg RNA. The percentage of SERCA3b (3.3%) is similar to that of SERCA2b while the last two other SERCA3 isoforms remained poorly express in the aorta.

3.2. Localization of SERCA isoforms expressed in normal murine cardiovascular tissues.

Confocal immunofluorescence confirmed distinct distribution of SERCA isoforms within cardiomyocytes and vascular cells (Fig. 2). As expected, SERCA2a was abundantly expressed in cardiomyocytes; in the coronary arteries, SERCA2a expression was barely detectable in vascular smooth muscle cells (VSMC) but substantial in endothelial cells (EC). Interestingly, in aorta samples, expression of SERCA2a, detected by immunofluorescence, was found in both vascular smooth muscle and endothelial cells (Fig. 3). The ubiquitous SERCA2b isoform was expressed at similar levels in every cell type (cardiomyocytes, VSMC and EC) (Figs. 2 & 3), whereas SERCA3a isoform seemed restricted to EC. Of note, low expression of SERCA3a was also detected in aortic VSMC (Fig. 3). In contrast, the SERCA3b isoform was strongly expressed in VSMC and hardly in EC (Figs. 2 & 3). Finally, SERCA3c isoform expression was faint in every cardiovascular cell type. Remarkably, in EC, ubiquitous isoform SERCA2b and SERCA3b were located in the basal part of the cell, whereas SERCA2a and SERCA3a were positioned in the luminal part (Fig. 2), supporting the functional association of SERCA2a and SERCA3a required for NO synthesis [19,24].

3.3. Alteration of expression and/or subcellular localization of SERCA isoforms in cardiomyocytes during heart failure

The heart failure model used was myocardial infarction (MI) induced by ligation of the left coronary artery in 2 month old C57BL6 mice. Progressive remodeling was evidenced by left ventricular (LV) dilation and deterioration of LV function at 1 and 6 months after infarction (Fig. 4A & Table 3). Six months after MI induction, heart weight and heart weight/body weight or heart weight/tibia length ratios were increased (Table 4). Furthermore, histological examination revealed an increase of the size of LV cardiomyocytes in MI mice (Fig. 4B) and fibrosis in the scarred area of the myocardial infarction (Fig. 4C).

In order to quantify mRNA expression, we first determined the rate of amplification for each cDNA (Supplementary data Fig. 1S). Next, we assessed SERCA isoform expression in the mouse model of heart failure using real-time RT-PCR analysis and confocal immunofluorescence microscopy (Fig. 5 & Table 2). Since a high level of fibrosis was observed in MI hearts, leading to a higher proportion of non-cardiomyocyte cells, we used the ubiquitous GAPDH gene and cardiomyocyte specific cardiac calsequestrin gene (CSQ) as reference gene since they have been shown to be stable in the course of hypertrophic remodeling [25]. As expected, the relative expression of SERCA2a transcripts was significantly decreased in failing hearts regardless of the reference gene used (Fig. 5A & B), whereas that of SERCA2b remained unchanged. Concerning the other SERCA isoform transcript expressions, a similar decrease of expression was observed for SERCA3b and 3c in failing hearts, while no significant differences were obtained for SERCA3a (Fig. 5C & D). These results were further confirmed for SERCA2 (a and b) isoforms at the protein level by western blot (Fig. 5E–G).

Cellular localization of SERCA isoforms within failing cardiomyocytes was assessed by confocal microscopy immunofluorescence (Fig. 5H). In sham cardiomyocytes, SERCA2a and SERCA2b demonstrated a similar

Table 2
Absolute quantification of different SERCA variants mRNA in normal and diseased cardiovascular tissues.

SERCA (pg/1 μg RNA)	Control heart ($n = 22$)	Failing heart ($n = 23$)	(Multiple comparison test) $P < 0.05$	WT aorta ($n = 9$)	ApoE ($^{-/-}$) aorta ($n = 8$)	(Multiple comparison test) $P < 0.05$
SERCA2a	919.4 ± 143.5	436.01 ± 61.6	***	27.90 ± 6.64	13.77 ± 0.81	*
SERCA2b	0.86 ± 0.17	0.64 ± 0.11	ns	1.59 ± 0.19	1.61 ± 0.20	ns
SERCA3a	0.003 ± 0.001	0.002 ± 0.0002	ns	0.016 ± 0.003	00.070 ± 0.025	*
SERCA3b	0.193 ± 0.08	0.028 ± 0.003	*	1.01 ± 0.21	1.42 ± 0.15	ns
SERCA3c	0.014 ± 0.005	0.003 ± 0.001	ns	0.11 ± 0.01	0.12 ± 0.01	ns

SERCA (%)	Control heart ($n = 22$)	Failing heart ($n = 23$)	WT aorta ($n = 9$)	ApoE ($^{-/-}$) aorta ($n = 8$)
SERCA2a	99.89	99.84	91.07	81.15
SERCA2b	0.093	0.146	5.19	9.47
SERCA3a	<0.001	<0.001	0.05	0.41
SERCA3b	0.021	0.006	3.30	8.28
SERCA3c	0.001	<0.001	0.38	0.69

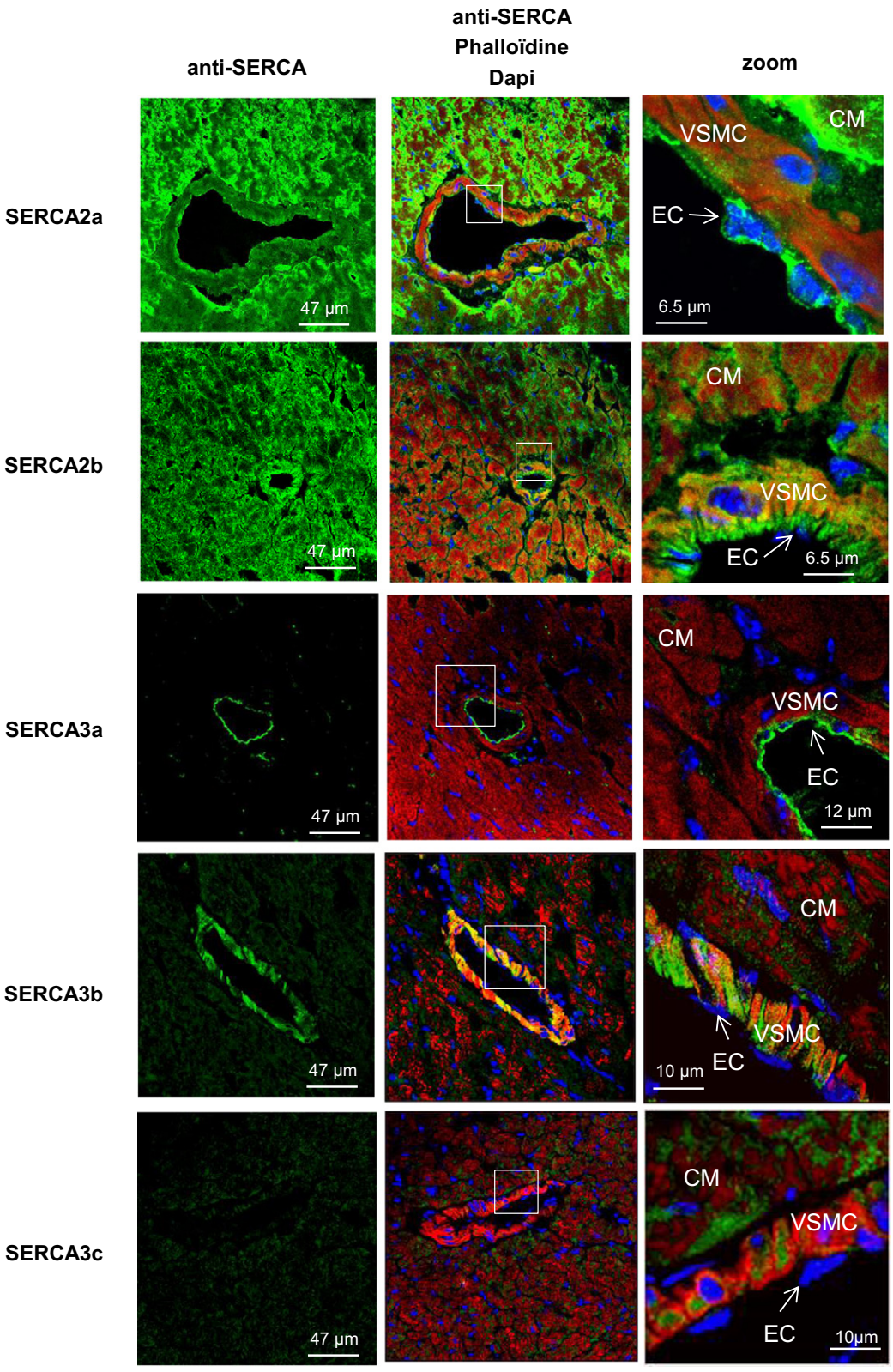

Fig. 2. Expression of SERCA isoforms in cardiovascular tissues and cells. **A.** Localization of SERCA isoforms in the left ventricle of normal mice by cell type. Confocal immunofluorescence microscopy with SERCA-specific antibodies (green) of left ventricle sections from normal mice. Red—F-actin, phalloidin. Nuclei were stained with Dapi (blue). Abbreviations: CM—cardiomyocytes; VSMC—vascular smooth muscle cells; EC—endothelial cells.

subcompartmental localization in the longitudinal reticulum, in opposite phase with the position of the Z-line, delineated by desmin staining (Fig. 5H). In marked contrast, both of these SERCA2 isoforms were co-localized with the Z-line area in failing cardiomyocytes, suggesting a re-localization of these two proteins from the longitudinal to the junctional reticulum.

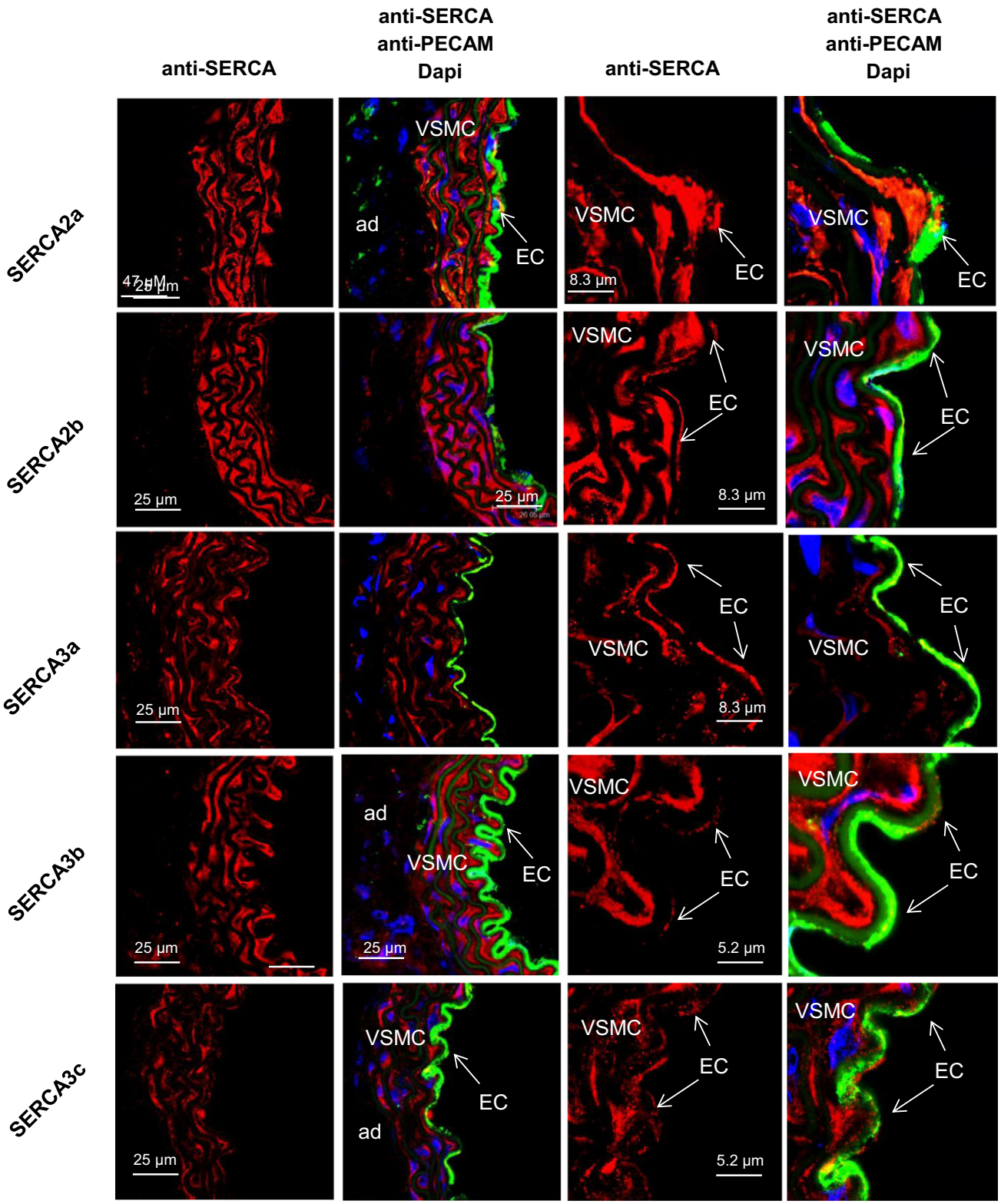

Fig. 3. Cell-specific expression of SERCA isoforms in normal mouse thoracic aorta. Confocal immunofluorescence with SERCA specific antibodies (red) of aorta sections from normal mice. Green—immunofluorescence with PECAM, a marker of endothelial cells. Nuclei were stained with Dapi (blue). Abbreviations: CM—cardiomyocytes; VSMC—vascular smooth muscle cells; EC—endothelial cells.

3.4. Alteration of expression and/or subcellular localisation of SERCA isoforms in vessels during atherosclerosis

We used hypercholesterolemic apolipoprotein$^{-/-}$ mice (ApoE$^{-/-}$) as a model of vascular remodeling (Fig. 6). Lesion development in the brachiocephalic artery of ApoE$^{-/-}$ mice was visualized by high-resolution ultrasound biomicroscopy. Plaque size significantly increased beginning at 42 weeks of age and continued to increase until the end of the study (Fig. 6A). Lesion surface area was greatest at 200 μm from the appearance of the first aortic valve cusp and

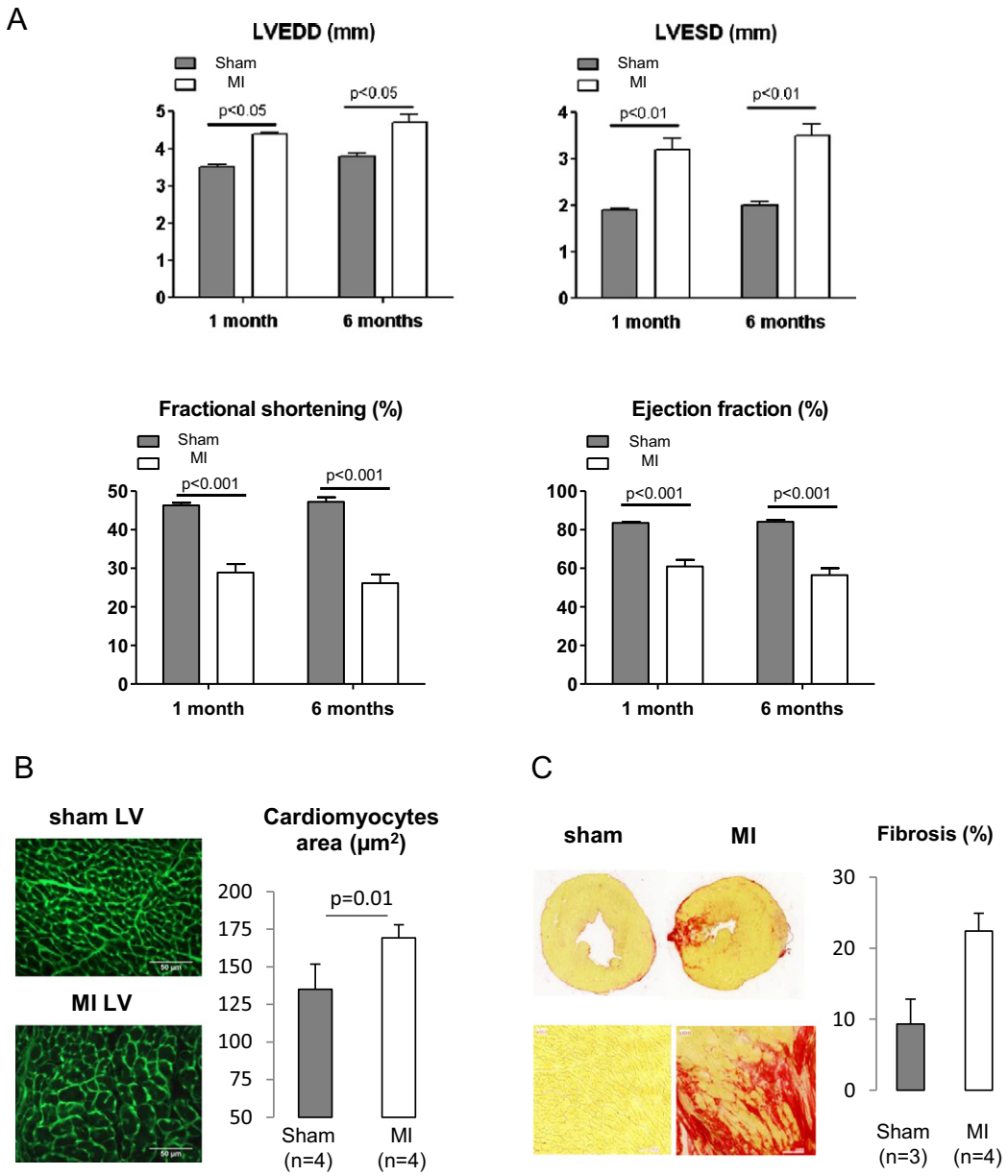

Fig. 4. Assessment of LV function, cardiomyocytes hypertrophy and myocardial fibrosis in MI hearts. **A.** Assessment of LV function using transthoracic echocardiography in sham operated and MI mice, 1 and 6 months after surgery. LVEDD: left ventricle end diastolic diameter; LVESD: left ventricle end systolic diameter. **B.** Analysis of cardiomyocytes sizes in sham and MI left ventricles. Left panel: Germ agglutinin staining. Right panel: Mean cardiomyocytes area in 4 sham- and 4 MI-operated animals. 250 individual measurements from 5 sections were performed for each animal. **C.** Sirius red staining of heart cross sections. Left panel: Representative image. Right panel: Relative quantification of fibrosis. Zone of infarction is included in the quantification.

Table 3
Assessment of cardiac function by transthoracic echography in sham operated and MI mice, 1 and 6 months after surgery.

	1 month after surgery			6 months after surgery		
	Sham operated ($n = 7$) Mean ± SD	MI ($n = 16$) Mean ± SD	p (t-test)	Sham operated ($n = 7$) Mean ± SD	MI ($n = 15$) Mean ± SD	p (t-test)
HR (b/min)	512.4 ± 9.7	483.0 ± 16.1	p = ns	531.2 ± 15.9	493.5 ± 15.9	p = ns
IVSDT (mm)	0.61 ± 0.01	0.51 ± 0.01	$p < 0.01$	0.67 ± 0.04	0.61 ± 0.02	p = ns
IVSST (mm)	1.04 ± 0.02	0.86 ± 0.04	$p < 0.05$	1.21 ± 0.004	0.92 ± 0.03	$p < 0.01$
PWDT (mm)	0.82 ± 0.03	0.61 ± 0.02	$p < 0.01$	0.90 ± 0.03	0.71 ± 0.03	$p < 0.01$
PWST (mm)	1.20 ± 0.05	0.95 ± 0.07	$p < 0.01$	1.35 ± 0.05	1.03 ± 0.05	$p < 0.01$
H/R (IVSDT + PWDT) / LVEDD	4.07 ± 0.14	2.65 ± 0.13	$p < 0.01$	4.10 ± 0.24	2.92 ± 0.18	$p < 0.01$

The following parameters were measured: IVSDT: interventricular septum diastolic thickness; IVSST: interventricular septum systolic thickness; LVEDD: left ventricle end diastolic diameter; LVESD: left ventricle end systolic diameter; PWDT; posterior wall diastolic thickness; PWST: posterior wall systolic thickness; EDV: end diastolic volume; ESV: end systolic volume; EF: ejection fraction; FR: fractional shortening; Ejct vol: ejection volume; HR: heart rate; h/r = (IVSDT + PWDT)/LVEDD.

Table 4
Morphometric analysis of sham operated and MI mice, 6 months after surgery.

	Sham operated ($n = 7$) Mean ± SD	MI ($n = 15$) Mean ± SD	p (t-test)
Body weight (g)	30.86 ± 0.34	30.67 ± 0.41	ns
Heart weight (mg)	155.30 ± 2.76	197.7 ± 11.21	$p < 0.001$
Tibia length (cm)	1.78 ± 0.02	1.79 ± 0.02	ns
Heart/body weight	5.04 ± 0.08	6.45 ± 0.37	$p < 0.001$
Heart/tibia length	87.01 ± 1.63	110.05 ± 5.977	$p < 0.001$

smallest at 800 μm, corresponding to the emergence of the aorta (Fig. 6B).

Given that the development of atherosclerotic lesions is associated with the trans-differentiation of VSMC from a contractile towards synthetic/proliferating/inflammatory phenotype [18,26], we first analyzed the expression of markers of phenotype and inflammation (Fig. 7A). The expressions of smooth muscle myosin heavy chain alpha (α-MHC), SM22 alpha (SM22) and smoothelin, all markers of contractile smooth muscle, were significantly decreased in thoracic aortas from ApoE$^{-/-}$ mice with atherosclerotic plaques (Fig. 7A). In contrast, the expression of E-selectin, a cell adhesion molecule expressed only in endothelial cells activated by cytokines and known to play an important role in the recruitment of these cells to inflammatory sites, was significantly increased in atherosclerotic vessels (Fig. 7A), confirming the phenotypic transition of VSMCs in thoracic aorta from ApoE$^{-/-}$ mice.

Pathological vascular remodeling in ApoE$^{-/-}$ mice was associated with a 2 fold decrease of the major isoform SERCA2a (Fig. 7B & Table 2). Furthermore, SERCA2b, SERCA3b and SERCA3c expressions were also decreased in atherosclerotic vessels (Fig. 7B & C; Table 2). Remarkably, the expression of SERCA3a isoform augmented 8 fold even if its percentage only reached 0.4% in ApoE$^{-/-}$ mice aorta (Fig. 7C; Table 2).

Histological analysis confirmed the presence of atherosclerotic lesions on aortic roots of all ApoE$^{-/-}$ animals; no lesions were observed in control mice (Fig. 6). The media area of aortic root atherosclerotic lesions, defined by elastin layers (Fig. 7D), was severely damaged and contained a large area composed of crowded elastic fibers lacking VSMC. Abundant neointima, defined as a layer within the internal elastic lamina (IEL) and lumen, was clearly identified in aortic roots from ApoE$^{-/-}$ animals. SERCA2a was expressed in both VSMC and EC of aortic roots (Fig. 7D), in agreement with our observations in coronary vessels and in the aorta (Fig. 2 & 3). As expected, SERCA3a expression was highest in the EC layer (Fig. 8D). SERCA2a expression was dramatically decreased in both neointima and media of atherosclerotic lesions in ApoE$^{-/-}$ mice. Nevertheless, SERCA2a was still detected in the luminal part of atherosclerotic vessels suggesting its expression in ECs. Furthermore, SERCA3a was abundantly expressed in the luminal part of the atherosclerotic vessels suggesting an enlargement of the endothelial cell layer. Large and round SERCA3a positive cells were also visualized in the neointima.

4. Discussion

We demonstrated the simultaneous expression of several SERCA isoforms with differential calcium affinity and pump activity in mouse cardiomyocytes, VSMC and endothelial cells and their dynamic variation and reorganization in disease states.

4.1. In mouse cardiomyocytes

The SERCA system is composed of at least 4 isoforms: SERCA 2a, 2b, 3b and 3c each with a specific intracellular location, as illustrated in Fig. 8A. In human heart, we previously described at least 6 SERCA isoforms: SERCA2a, 2b, 2c and SERCA3a, 3d and 3f [1,22].

We, and others [1,15], using relative mRNA quantification, have identified SERCA2a as the major cardiac isoform and SERCA2b as a minor cardiac isoform. Here, we observed a global reduction of both SERCA2 and SERCA3 expression in our pathological model. We also report that even though SERCA2a is down-regulated during pathologic cardiac hypertrophy and heart failure, its relative expression remains largely predominant. Observation from previous works from transgenic mice clearly suggested that the level of SERCA2a expression is critical. Wuytack et al. have produced transgenic mice in which SERCA2a was replaced by SERCA2b, resulting in cardiac dysfunction and hypertrophy [27], showing that the high Ca^{2+} affinity SERCA2b isoforms appeared to be an inadequate substitute for SERCA2a. The total level of SERCA2 was lower in SERCA2a-deficient mice in an initial study, but further overexpression of SERCA2b in these cardiomyocytes led to increased SR calcium transport and enhanced mechanical function (contractility and relaxation), without preventing cardiac hypertrophy [15] or fibrosis [4]. Althought, a spontaneous two-fold increase in cardiac phospholamban expression might counteract a possible effect of SERCA2b [27]. Interestingly, SERCA2b/WT heterozygous mice in which the natural SERCA2a isoform is the major isoform do not present hypertrophy, confirming that SERCA2a is necessary and most likely sufficient.

Reduced SERCA2a activity and SR Ca^{2+} uptake lead to abnormal Ca^{2+} handling in failing cardiomyocytes including an increase in diastolic Ca^{2+}, abnormally long time course of Ca^{2+} transients, and decrease in SR Ca^{2+} release [28]. Furthermore, reduction of SERCA2a expression by RNA silencing in cardiac myocytes resulted in increased expression of transient receptor potential channels (TRPC) and activation of the calcium/calcineurin-dependent complex [29]. These Ca^{2+}-dependent signaling pathways initiate and sustain hypertrophic growth and remodeling, which often progress to heart failure [20,28]. By lowering cytosolic Ca^{2+}, SERCA2a expression inhibits calcineurin activity and associated hypertrophic and apoptotic signaling pathways [30].

Similarly to what was described in human cardiomyocytes, both SERCA2a and SERCA2b proteins were targeted to the same subcellular regions (longitudinal SR) [1,4,31]. In the normal condition, SERCA2 proteins were found in opposite phase to the position of the I-band, in the SR wrapping myofilaments. This is consistent with the SR being the source of large Ca^{2+} mobilization into the cytosol, during cardiac excitation–contraction coupling, essential to produce a rapid increase in cytosolic [Ca^{2+}] responsible for activation of the myofilaments to be translated into a proper twitch contraction. The rate of the rise of cytosolic Ca^{2+} depends on the triggering and gating of the RyR and the amount of Ca^{2+} available in SR for release [32].

We have found that in cardiomyocytes from failing hearts, SERCA2 proteins relocated to the Z-line (Fig. 8B). The Z line is closer to extracellular exchange area (T-tubule) and contains LTCC and RyR channels. The LTCCs and RyR form couplons at the interface between the sarcolemma and the junctional SR. A defective coupling of Ca^{2+} influx via LTCC, preventing the activation of RyR, has been implicated in a reduced SR Ca^{2+} release in heart failure. Both functional changes in LTCC properties and structural re-organization of this L-type channel within T-tubules could be involved [33]. Relocation of SERCA2 to the Z-line in hypertrophied myocytes might be associated to T-tubule disorganization shown to coincide with myocardial dysfunction and calcium transient abnormalities in hypertensive rats [34] and suggest a compensation of defective LTCC/RyR coupling by rising available SR Ca^{2+} content.

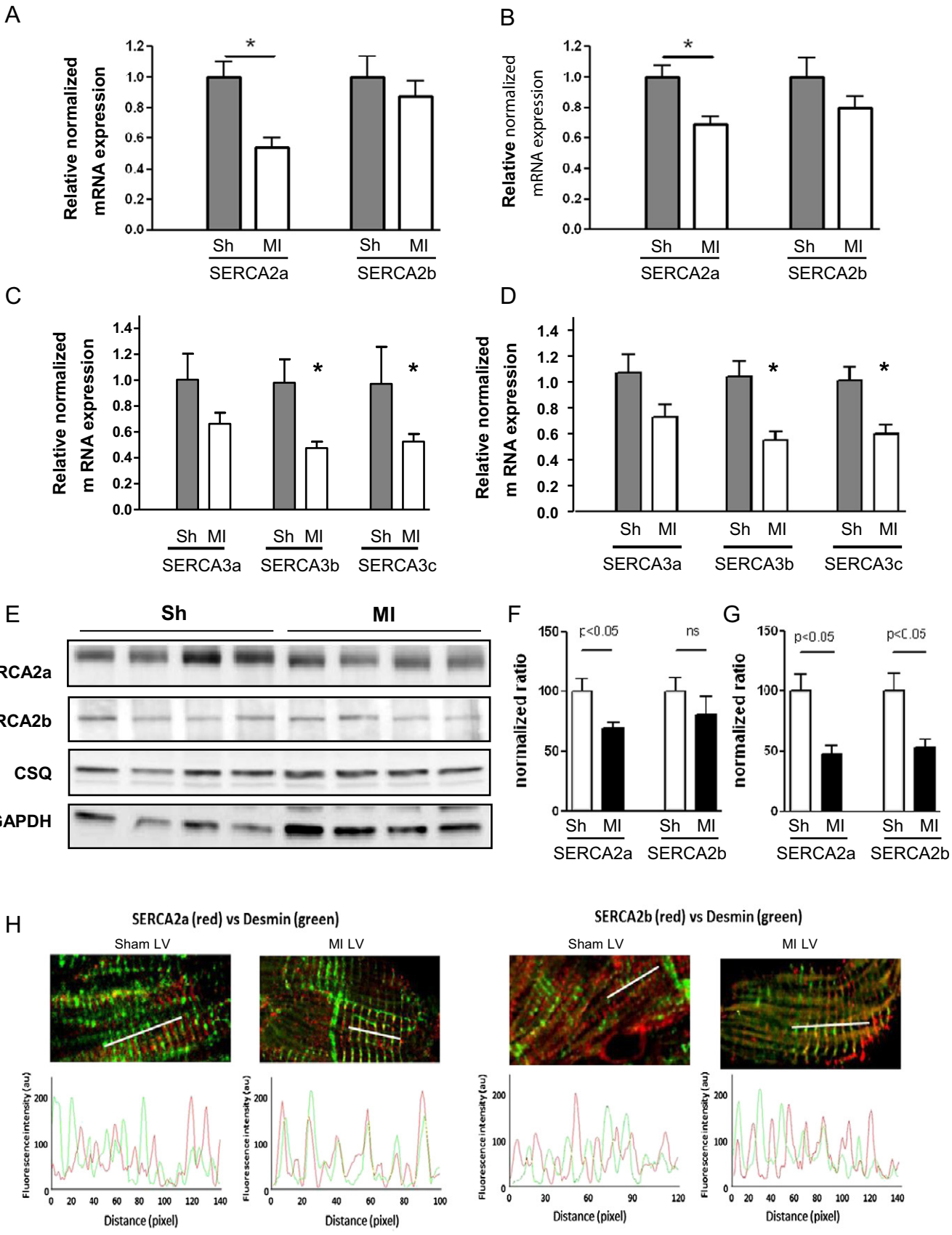

Fig. 5. Alteration of SERCA isoform expression in the failing heart. Relative expression of SERCA 2a and 2b variants in sham- ($n = 9$) and MI- ($n = 20$) operated animals normalized on calsequestrin (CSQ) (**A**) and GAPDH (**B**). Relative expression of SERCA 3a, 3b and 3c variants in sham- ($n = 12$) and MI- ($n = 20$) operated animals normalized on calsequestrin (CSQ) (**C**) and GAPDH (**D**). **E.** Immunoblot analysis (left panel) and bar-graph representing normalized relative quantification of SERCA2a and SERCA2b expression in sham-operated and MI animals. **F.** Localization of SERCA2a and SERCA2b within cardiomyocytes from sham (left panel) and MI (right panel) mouse hearts. **Upper panel:** Confocal microscopy immunofluorescence with a-SERCA (red) and a-desmin (green) antibodies on transverse sections. **Lower panel:** Analysis of SERCA and desmin colocalization in normal and failing cardiomyocytes.

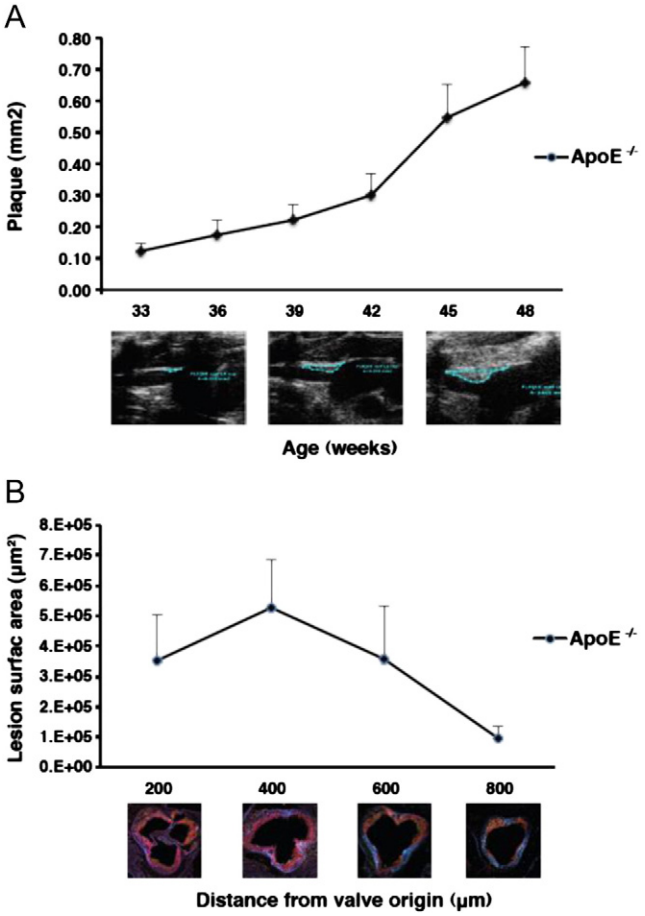

Fig. 6. Atherosclerotic plaques in aged ApoE ($^{-/-}$) mice. **A.** Lesion development in the brachiocephalic artery of ApoE KO mice visualized by high-resolution ultrasound biomicroscopy (UBM). Lesion size (y axis, mm^2) was measured for every mouse at all time points examined. The study began at 33 weeks of age and images were taken every 3 weeks until the end of the study at 48 weeks of age. The ultrasound images underneath the graph represent plaque development at 33, 39 and 48 weeks of age. The atherosclerotic plaques are contoured in white lines. Plaque surface area was calculated by the VEVO software. **B.** Quantification of atherosclerotic lesion surface area in the aortic roots of ApoE KO mice. Lipid content was quantified on aortic root cryosections from 48 week old mice stained with oil red O and analyzed under polarized light. The distance from the valve origin represents 200, 400, 600, and 800 μm from the appearance of the first aortic valve cusp; 800 μm is the emergence of the aorta (800 μm). $n = 6$.

Remarkably, relocation of SERCA2 from the SR wrapping myofilaments might result in slow rise Ca^{2+} influx across the sarcolemma ensuing in inefficient contraction.

The mouse SERCA system expressed in the heart is also distinct from the human one, as no SERCA2c mRNA was found in mice. While the role played by SERCA2C in human heart remained to be clarified, its specific localization to longitudinal SR and intercalated discs in close proximity to the sarcolemma, an area that could display relatively high calcium concentration, was in agreement with its lower apparent affinity for Ca^{2+}. Such localization was not observed for SERCA expressed in mouse cardiomyocyte. But it is possible that some function associated to SERCA2c in human heart could be done by SERCA3b which also share similar affinity for Ca^{2+}.

Among SERCA3 isoforms, only SERCA3b was clearly identified in mouse cardiomyocytes by its specific location at the junctional SR, near the T-tubules, which corresponds to the localization of SERCA3a in human cardiomyocytes [1]. It is tempting to imagine that this area is more adapted to the SERCA3 protein as it can be richer in Ca^{2+} (due to its interaction with the extracellular medium), considering that SERCA3 works at a higher Ca^{2+} concentration than SERCA2 isoforms.

Limited data are available on human failing cardiac tissue, in which only a significant increase in SERCA3f was recently demonstrated, in addition to the well-established decrease in SERCA2a [1]. While the SR regulates excitation–contraction coupling due to its special ability to store calcium, the role of the ER in protein synthesis and processing and the disruption of such processes in pathologic situations (known as ER stress) is of growing importance in cardiomyocyte and in heart failure [1]. In this regard, an interesting connection can be made between 1) the increased expression of SERCA3f in human heart failure with a parallel increase in ER stress markers [22], and 2) the ability of SERCA3f to induce ER stress and apoptosis in HEK-293 cells [35]. SERCA3f and SERCA3b share the same C-terminal end and SERCA3b was also able to induce ER stress in human cells. However, it is not clear whether SERCA3b can be seen as an equivalent of SERCA3f in mice, as it is down-regulated in heart failure while SERCA3f expression was described to increase.

4.2. In vascular smooth muscle cells

The SERCA system is composed of at least 4 isoforms: SERCA 2a, 2b, 3b and 3c. As opposed to previous studies [16], SERCA2a was identified as a major isoform in both contractile and synthetic VSMC using the method of absolute mRNA quantification. Technical differences may account for the different results. This finding is novel but not surprising taking into account that synthetic VSMCs are able to produce tonic contraction (rev. [18,19]). In VSMCs, oscillatory type of Ca^{2+} transients triggers phasic contraction, typical of coronary and low resistance arteries highly expressing SERCA2a. Tonic contractions observed in large arteries and veins are driven by the steady-state increase in cytosolic Ca^{2+}, observed also in synthetic VSMC (rev. [18,19]). Several observations support the evidence that the calcium response shape appears to be dependent on SERCA2a expression: 1) blocking SERCA activity also strongly inhibits the Ca^{2+} oscillations, demonstrating that they are caused by release of Ca^{2+} from the SR [36–38]; 2) trans-differentiation of VSMC towards synthetic phenotype is associated with a loss of both Ca^{2+} oscillations and SERCA2a expression (this paper and [39,40]; and 3) SERCA2a gene transfer to synthetic cultured VSMC modifies the agonist-induced calcium transient from steady-state to oscillatory mode [41]. Importantly, restoring SERCA2a expression by gene transfer in synthetic cultured VSMC also inhibits Ca^{2+} dependent activation of transcription factor NFAT required for proliferation and migration of VSMC [30,41,42].

We also report a relatively high expression of the SERCA3b isoform in mouse VSMC, similar to one of the ubiquitous SERCA2b isoform. In humans, SERCA3b have been found highly expressed in the lung, kidney and pancreas; however its cellular localization and specific function have not yet been investigated [19]. The fact that SERCA3b expression appears to be important in normal VSMC and its specific localization in cardiomyocytes at the junctional SR near T tubules suggests that it could be involved in interaction with extracellular Ca^{2+} influx.

4.3. In endothelial cells

The SERCA system is composed of at least 5 isoforms: SERCA2a, 2b, 3a as well as the slightly expressed 3b and 3c. First, we have detected a strong expression of SERCA3a in EC, confirming previous observations describing SERCA3a as a major endothelial-specific isoform [43]. Second, according to immunolabeling data, SERCA2a appears to be a major isoform co-expressed with SERCA3a in the luminal part of EC. This latter observation is consistent with the described role of SERCA3a and SERCA2a in EC related to the regulation of NO synthesis from L-arginine by the nitric oxide synthase (eNOS, endothelial nitric oxide synthase) (rev in [19,44]). Several observations support the cooperative action of SERCA2a and SERCA3a in the control of NO production

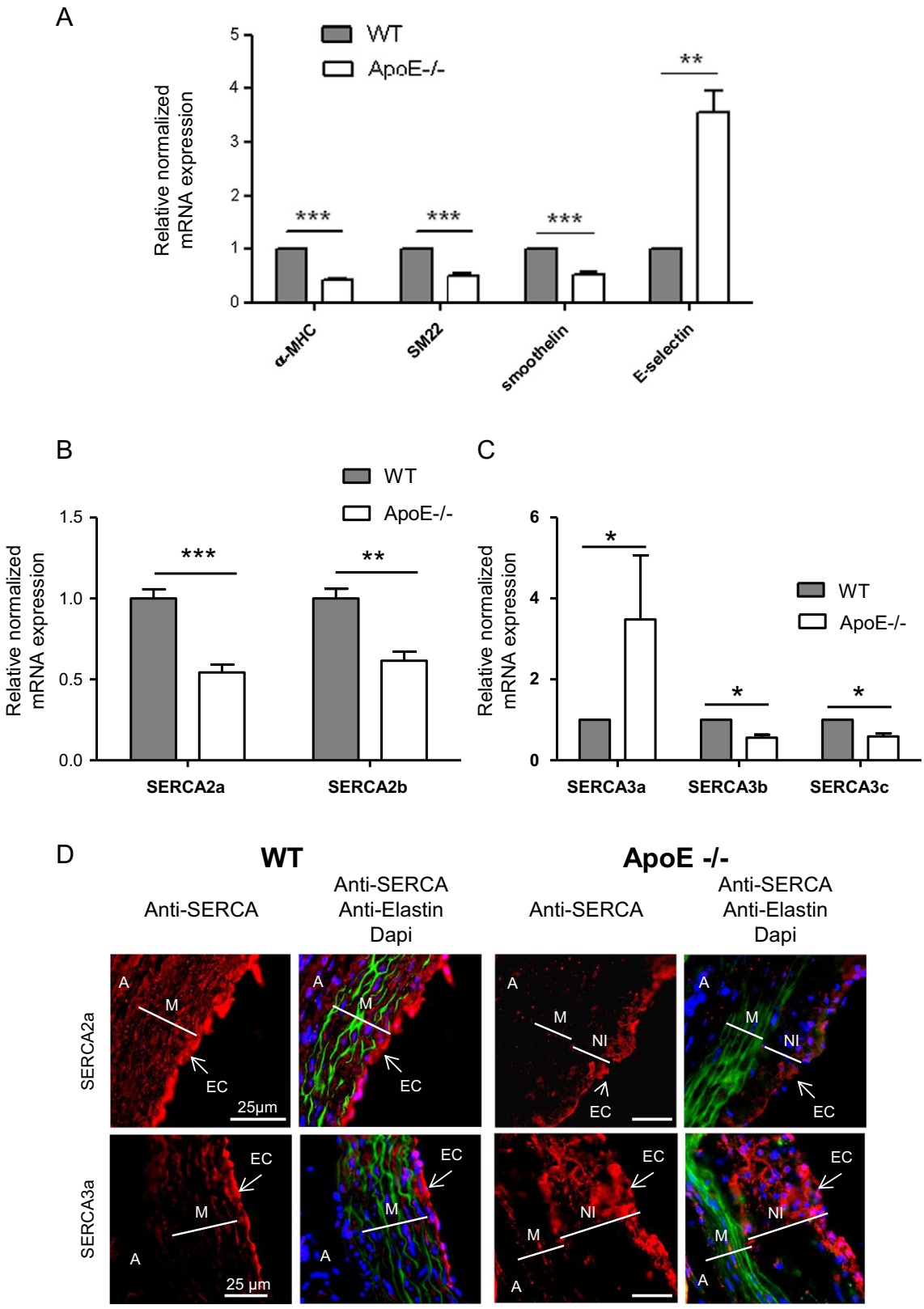

Fig. 7. Alteration of SERCA isoforms expression in atherosclerotic vessels. **A.** Real-time RT-PCR analysis of makers of contractile VSMC and inflammation in WT ($n = 7$) and MI ($n = 4$) animals. **B & C.** Real-time RT-PCR analysis of SERCA2 and SERCA3 family members expression in WT ($n = 7$) and MI ($n = 4$) animals. **D**. Immunofluorescence with SERCA specific antibodies (red) of aorta root sections from normal and ApoE$^{-/-}$ mice. Green—elastin autofluorescence. Nuclei were stained with Dapi (blue). Abbreviations: A—adventitia, M—media, NI—neointima, and EC—endothelial cells.

in EC: 1) ablation of SERCA3 genes results in defective nitric oxide (NO) synthesis [45]; 2) SERCA2a and SERCA3a colocalize with eNOS and caveolin in sub-plasma membrane reticulum in EC [19,24]; and 3) overexpression of SERCA2a in human EC, resulting in increased ER Ca^{2+} storage and mobilization, also enhances eNOS activity and cGMP production [24].

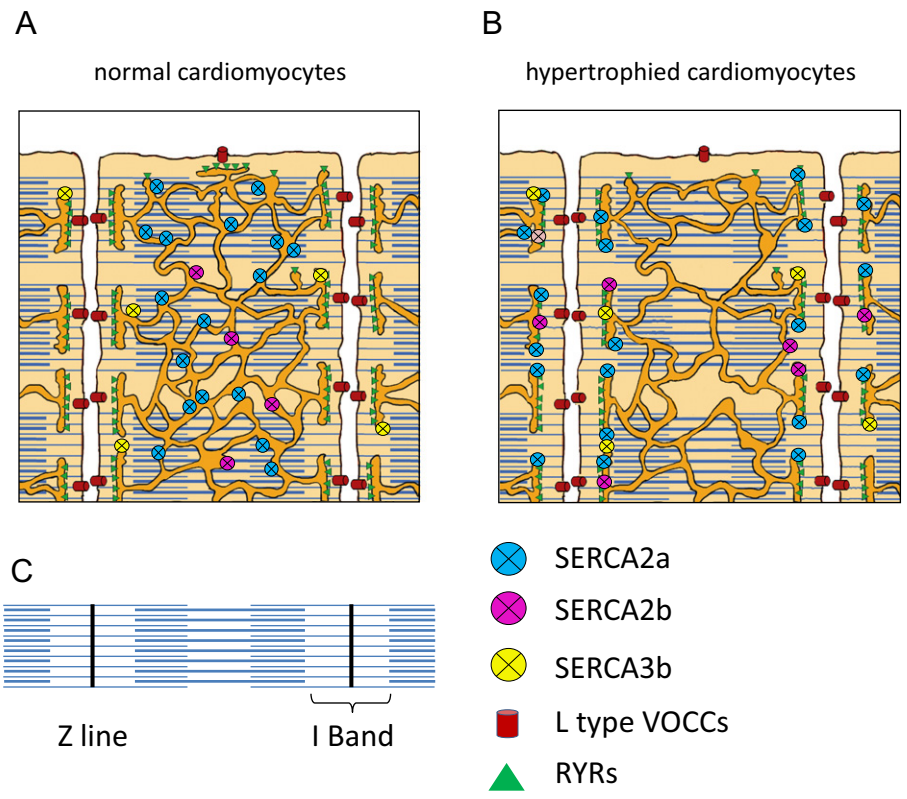

Fig. 8. Schematic localization of SERCA isoforms in normal and hypertrophied cardiomyocytes. Schematic representations of the structure of normal (Panel A) and failing (Panel B) cardiac myocytes illustrate the relative position of the SERCA isoforms on the SR network that wrap around the myofibrils. Panel C shows the topology of a myofibril.

We report an increase in SERCA3a expression in atherosclerotic vessels, together with a modification of the pattern of expression. The increase in SERCA3a expression might compensate the decrease of SERCA2a. However, the SERCA3a expression appears more diffuse at the atherosclerosis site compared to its normal localization. Given the fact that SERCA3a is preferentially expressed by endothelial cells and blood cells [46,47], it is interesting to suggest that SERCA3a expression indicates the infiltration of endothelial cells precursors or monocytes in the neointima of atherosclerotic vessels, as it is described (intimal hyperplasia in murine models [48].

5. Conclusions

The simultaneous expression of several SERCA isoforms in cardiovascular cells enlightens possible functions for each of the SERCA isoforms, given the specific expression and localization. Data obtained in a particular set of pathological conditions revealed specific regulation of SERCA isoforms, suggesting that not only the variety, but also the combination of SERCA isoforms achieves tight regulation of cellular functions. We have identified SERCA2a as the major isoform in both cardiac and vascular myocytes, in normal and pathological conditions. The expression of SERCA2a mRNA is ~30 fold higher in the heart compared to vascular tissues, in conformity with highest impact of contractile function in cardiomyocyte physiology. Notably, nearly half the amount of SERCA2a mRNA is measured in both failing cardiomyocytes and synthetic VSMCs compared to healthy tissues. Our study shows that the SERCA2a isoform is the principal regulator of excitation–contraction coupling in both CMs and contractile VSMCs and supports a dynamic and integrated regulation of the SERCA isoform system. The roles of previously unexplored isoforms, along with the dynamic interactions between isoforms, deserve further studies.

Supplementary data to this article can be found online at http://dx.doi.org/10.1016/j.bbamcr.2014.08.002.

Acknowledgements

This study was supported by grants from the INSERM, Ministère de la Recherche, DHU Ageing Thorax-Vessels-Blood (A-TVB), ANR Grant 11 BSV1 034 01, Association Française contre les Myopathies (AFM 14048, AFM 16442), and Fondation Cœur-poumon. Dr Hajjar was supported by NIH grants R01 HL117505, HL093183, and P50 HL112324.

References

[1] S. Dally, E. Corvazier, R. Bredoux, R. Bobe, J. Enouf, Multiple and diverse coexpression, location, and regulation of additional SERCA2 and SERCA3 isoforms in nonfailing and failing human heart, J. Mol. Cell. Cardiol. 48 (2010) 633–644.
[2] T. Seidler, G. Hasenfuss, L.S. Maier, Targeting altered calcium physiology in the heart: translational approaches to excitation, contraction, and transcription, Physiology (Bethesda) 22 (2007) 328–334.
[3] M. Periasamy, A. Kalyanasundaram, SERCA pump isoforms: their role in calcium transport and disease, Muscle Nerve 35 (2007) 430–442.
[4] A.L. Greene, M.J. Lalli, Y. Ji, G.J. Babu, I. Grupp, M. Sussman, M. Periasamy, Overexpression of SERCA2b in the heart leads to an increase in sarcoplasmic reticulum calcium transport function and increased cardiac contractility, J. Biol. Chem. 275 (2000) 24722–24727.
[5] F. Wuytack, B. Papp, H. Verboomen, L. Raeymaekers, L. Dode, R. Bobe, J. Enouf, S. Bokkala, K.S. Authi, R. Casteels, A sarco/endoplasmic reticulum Ca^{2+}ATPase 3-type Ca^{2+} pump is expressed in platelets, in lymphoid cells, and in mast cells, J. Biol. Chem. 269 (1994) 1410–1416.
[6] V. Martin, R. Bredoux, E. Corvazier, R. Van Gorp, T. Kovacs, P. Gelebart, J. Enouf, Three novel sarco/endoplasmic reticulum Ca^{2+}ATPase (SERCA) 3 isoforms. Expression, regulation, and function of the membres of the SERCA3 family, J. Biol. Chem. 277 (2002) 24442–24452.
[7] R. Bobe, R. Bredoux, E. Corvazier, J.P. Andersen, J.D. Clausen, L. Dode, T. Kovacs, J. Enouf, Identification, expression, function, and localization of a novel (sixth) isoform of the human sarco/endoplasmic reticulum Ca^{2+}ATPase 3 gene, J. Biol. Chem. 279 (2004) 24297–24306.
[8] P.D. Borge Jr., B.A. Wolf, Insulin receptor substrate 1 regulation of sarco-endoplasmic reticulum calcium ATPase 3 in insulin-secreting beta-cells, J. Biol. Chem. 278 (2003) 11359–11368.
[9] V. Martin, R. Bredoux, E. Corvazier, B. Papp, J. Enouf, Platelet Ca^{2+}ATPases: a plural, species-specific, and multiple hypertension-regulated expression system, Hypertension 35 (2000) 91–102.

[10] H. Verboomen, F. Wuytack, H.D. Smedt, B. Himpens, R. Casteels, Functional difference between SERCA2a and SERCA2b Ca^{2+} pumps and their modulation by phospholamban, Biochem. J. 286 (1992) 591–596.
[11] S. Dally, R. Bredoux, E. Corvazier, J.P. Andersen, J.D. Clausen, L. Dode, M. Fanchaouy, P. Gelebart, V. Monceau, F. Del Monte, J.K. Gwathmey, R. Hajjar, C. Chaabane, R. Bobe, A. Raies, J. Enouf, Ca^{2+}ATPases in non-failing and failing heart: evidence for a novel cardiac sarco/endoplasmic reticulum Ca^{2+}ATPase 2 isoform (SERCA2c), Biochem. J. 395 (2006) 249–258.
[12] J. Lytton, M. Westlin, S.E. Burk, G.E. Shull, D.H. MacLennan, Functional comparisons between isoforms of the sarcoplasmic or endoplasmic reticulum family of calcium pumps, J. Biol. Chem. 267 (1992) 14483–14489.
[13] S.L. Dodd, T.J. Koesterer, Clenbuterol attenuates muscle atrophy and dysfunction in hindlimb-suspended rats, Aviat. Space Environ. Med. 73 (2002) 635–639.
[14] E.R. Chemaly, R. Bobe, S. Adnot, R.J. Hajjar, L. Lipskaia, Sarco (Endo) plasmic Reticulum Calcium ATPases (SERCA) isoforms in the normal and diseased cardiac, vascular and skeletal muscle systems, J. Cardiovasc. Dis. Diagn. 1 (2013) 6.
[15] P. Vangheluwe, M. Schuermans, L. Raeymaekers, F. Wuytack, Tight interplay between the Ca^{2+} affinity of the cardiac SERCA2 Ca^{2+} pump and the SERCA2 expression level, Cell Calcium 42 (2007) 281–289.
[16] D.O. Levitsky, M. Clergue, F. Lambert, M.V. Souponitskaya, T.H. Le Jemtel, Y. Lecarpentier, A.M. Lompre, Sarcoplasmic reticulum calcium transport and $Ca^{(2+)}$-ATPase gene expression in thoracic and abdominal aortas of normotensive and spontaneously hypertensive rats, J. Biol. Chem. 268 (1993) 8325–8331.
[17] A.M. Lompre, R.J. Hajjar, S.E. Harding, E.G. Kranias, M.J. Lohse, A.R. Marks, Ca^{2+} cycling and new therapeutic approaches for heart failure, Circulation 121 (2010) 822–830.
[18] L. Lipskaia, I. Limon, R. Bobe, H. R, Calcium cycling in synthetic and contractile phasic or tonic vascular smooth muscle cells, in: S.H. InTech (Ed.), Current Basic and Pathological Approaches to the Function of Muscle Cells and Tissues—From Molecules to Humans, 2012.
[19] L. Lipskaia, L. Hadri, P. Le Prince, B. Esposito, F. Atassi, L. Liang, M. Glorian, I. Limon, A.M. Lompre, S. Lehoux, R.J. Hajjar, SERCA2a gene transfer prevents intimal proliferation in an organ culture of human internal mammary artery, Gene Ther. 20 (2013) 396–406.
[20] L. Lipskaia, E.R. Chemaly, L. Hadri, A.M. Lompre, R.J. Hajjar, Sarcoplasmic reticulum $Ca^{(2+)}$ ATPase as a therapeutic target for heart failure, Expert. Opin. Biol. Ther. 10 (2010) 29–41.
[21] V. Kairouz, L. Lipskaia, R.J. Hajjar, E.R. Chemaly, Molecular targets in heart failure gene therapy: current controversies and translational perspectives, Ann. N. Y. Acad. Sci. 1254 (2012) 42–50.
[22] S. Dally, V. Monceau, E. Corvazier, R. Bredoux, A. Raies, R. Bobe, F. del Monte, J. Enouf, Compartmentalized expression of three novel sarco/endoplasmic reticulum Ca^{2+}ATPase 3 isoforms including the switch to ER stress, SERCA3f, in non-failing and failing human heart, Cell Calcium 45 (2009) 144–154.
[23] K.J. Livak, T.D. Schmittgen, Analysis of relative gene expression data using real-time quantitative PCR and the 2(−Delta Delta C(T)) Method, Methods 25 (2001) 402–408.
[24] L. Hadri, R. Bobe, Y. Kawase, D. Ladage, K. Ishikawa, F. Atassi, D. Lebeche, E.G. Kranias, J.A. Leopold, A.M. Lompre, L. Lipskaia, R.J. Hajjar, SERCA2a gene transfer enhances eNOS expression and activity in endothelial cells, Mol. Ther. 18 (2010) 1284–1292.
[25] N.R. DiPaola, W.E. Sweet, L.B. Stull, G.S. Francis, C. Schomisch Moravec, Beta-adrenergic receptors and calcium cycling proteins in non-failing, hypertrophied and failing human hearts: transition from hypertrophy to failure, J. Mol. Cell. Cardiol. 33 (2001) 1283–1295.
[26] L. Lipskaia, L. Hadri, J.J. Lopez, R.J. Hajjar, R. Bobe, Benefit of SERCA2a gene transfer to vascular endothelial and smooth muscle cells: a new aspect in therapy of cardiovascular diseases, Curr. Vasc. Pharmacol. 11 (2013) 465–479.
[27] M. Ver Heyen, S. Heymans, G. Antoons, T. Reed, M. Periasamy, B. Awede, J. Lebacq, P. Vangheluwe, M. Dewerchin, D. Collen, K. Sipido, P. Carmeliet, F. Wuytack, Replacement of the muscle-specific sarcoplasmic reticulum $Ca^{(2+)}$-ATPase isoform SERCA2a by the nonmuscle SERCA2b homologue causes mild concentric hypertrophy and impairs contraction-relaxation of the heart, Circ. Res. 89 (2001) 838–846.
[28] A.R. Marks, Calcium cycling proteins and heart failure: mechanisms and therapeutics, J. Clin. Invest. 123 (2013) 46–52.
[29] M. Seth, C. Sumbilla, S.P. Mullen, D. Lewis, M.G. Klein, A. Hussain, J. Soboloff, D.L. Gill, G. Inesi, Sarco(endo)plasmic reticulum Ca^{2+}ATPase (SERCA) gene silencing and remodeling of the Ca^{2+} signaling mechanism in cardiac myocytes, Proc. Natl. Acad. Sci. U. S. A. 101 (2004) 16683–16688.
[30] L. Lipskaia, F. del Monte, T. Capiod, S. Yacoubi, L. Hadri, M. Hours, R.J. Hajjar, A.M. Lompre, Sarco/endoplasmic reticulum Ca^{2+}-ATPase gene transfer reduces vascular smooth muscle cell proliferation and neointima formation in the rat, Circ. Res. 97 (2005) 488–495.
[31] P. Vangheluwe, W.E. Louch, M. Ver Heyen, K. Sipido, L. Raeymaekers, F. Wuytack, Ca^{2+} transport ATPase isoforms SERCA2a and SERCA2b are targeted to the same sites in the murine heart, Cell Calcium 34 (2003) 457–464.
[32] D.M. Bers, Cardiac excitation–contraction coupling, Nature 415 (2002) 198–205.
[33] V. Bito, F.R. Heinzel, L. Biesmans, G. Antoons, K.R. Sipido, Crosstalk between L-type Ca^{2+} channels and the sarcoplasmic reticulum: alterations during cardiac remodelling, Cardiovasc. Res. 77 (2008) 315–324.
[34] S.J. Shah, G.L. Aistrup, D.K. Gupta, M.J. O'Toole, A.F. Nahhas, D. Schuster, N. Chirayil, N. Bassi, S. Ramakrishna, L. Beussink, S. Misener, B. Kane, D. Wang, B. Randolph, A. Ito, M. Wu, L. Akintilo, T. Mongkolrattanothai, M. Reddy, M. Kumar, R. Arora, J. Ng, J.A. Wasserstrom, Ultrastructural and cellular basis for the development of abnormal myocardial mechanics during the transition from hypertension to heart failure, Am. J. Physiol. Heart Circ. Physiol. 306 (2014) H88–H100.
[35] C. Chaabane, E. Corvazier, R. Bredoux, S. Dally, A. Raies, A. Villemain, E. Dupuy, J. Enouf, R. Bobe, Sarco/endoplasmic reticulum Ca^{2+} ATPase type 3 isoforms (SERCA3b and SERCA3f): distinct roles in cell adhesion and ER stress, Biochem. Biophys. Res. Commun. 345 (2006) 1377–1385.
[36] I.S. Bartlett, G.J. Crane, T.O. Neild, S.S. Segal, Electrophysiological basis of arteriolar vasomotion in vivo, J. Vasc. Res. 37 (2000) 568–575.
[37] R.E. Haddock, C.E. Hill, Differential activation of ion channels by inositol 1,4,5-trisphosphate (IP3)- and ryanodine-sensitive calcium stores in rat basilar artery vasomotion, J. Physiol. 545 (2002) 615–627.
[38] R.E. Haddock, G.D. Hirst, C.E. Hill, Voltage independence of vasomotion in isolated irideal arterioles of the rat, J. Physiol. 540 (2002) 219–229.
[39] L. Lipskaia, M.L. Pourci, C. Delomenie, L. Combettes, D. Goudouneche, J.L. Paul, T. Capiod, A.M. Lompre, Phosphatidylinositol 3-kinase and calcium-activated transcription pathways are required for VLDL-induced smooth muscle cell proliferation, Circ. Res. 92 (2003) 1115–1122.
[40] O. Vallot, L. Combettes, P. Jourdon, J. Inamo, I. Marty, M. Claret, A.M. Lompre, Intracellular $Ca^{(2+)}$ handling in vascular smooth muscle cells is affected by proliferation, Arterioscler. Thromb. Vasc. Biol. 20 (2000) 1225–1235.
[41] R. Bobe, L. Hadri, J.J. Lopez, Y. Sassi, F. Atassi, I. Karakikes, L. Liang, I. Limon, A.M. Lompre, S.N. Hatem, R.J. Hajjar, L. Lipskaia, SERCA2a controls the mode of agonist-induced intracellular Ca^{2+} signal, transcription factor NFAT and proliferation in human vascular smooth muscle cells, J. Mol. Cell. Cardiol. 50 (2011) 621–633.
[42] E. Merlet, L. Lipskaia, A. Marchand, L. Hadri, N. Mougenot, F. Atassi, L. Liang, S.N. Hatem, R.J. Hajjar, A.M. Lompre, A calcium-sensitive promoter construct for gene therapy, Gene Ther. 20 (2013) 248–254.
[43] I.I. Mountian, F. Baba-Aissa, J.C. Jonas, S. Humbert De, F. Wuytack, J.B. Parys, Expression of $Ca^{(2+)}$ transport genes in platelets and endothelial cells in hypertension, Hypertension 37 (2001) 135–141.
[44] J. Kao, C.N. Fortner, L.H. Liu, G.E. Shull, R.J. Paul, Ablation of the SERCA3 gene alters epithelium-dependent relaxation in mouse tracheal smooth muscle, Am. J. Physiol. 277 (1999) L264–L270.
[45] L.H. Liu, R.J. Paul, R.L. Sutliff, M.L. Miller, J.N. Lorenz, R.Y. Pun, J.J. Duffy, T. Doetschman, Y. Kimura, D.H. MacLennan, J.B. Hoying, G.E. Shull, Defective endothelium-dependent relaxation of vascular smooth muscle and endothelial cell Ca^{2+} signaling in mice lacking sarco(endo)plasmic reticulum Ca^{2+}ATPase isoform 3, J. Biol. Chem. 272 (1997) 30538–30545.
[46] I. Machuca, C. Domenget, P. Jurdic, Identification of avian sarcoplasmic reticulum $Ca^{(2+)}$-ATPase (SERCA3) as a novel 1,25(OH)(2)D(3) target gene in the monocytic lineage, Exp. Cell Res. 250 (1999) 364–375.
[47] T. Kovacs, F. Felfoldi, B. Papp, K. Paszty, R. Bredoux, A. Enyedi, J. Enouf, All three splice variants of the human sarco/endoplasmic reticulum Ca^{2+}ATPase 3 gene are translated to proteins: a study of their co-expression in platelets and lymphoid cells, Biochem. J. 358 (2001) 559–568.
[48] D.Y. Hui, Intimal hyperplasia in murine models, Curr. Drug Targets 9 (2008) 251–260.